

STABILITY OF VISCOELASTIC FILAMENTS: COMPARISON OF CONSTITUTIVE MODELS

David O. Olagunju ¹
Department of Mathematical Sciences
University of Delaware
Newark, DE 19716

July 23, 1999

¹This research was supported in part by NSF Grant No. DMS-9704622

Abstract

A thin filament model is used to analyze the stability of a viscoelastic thread subject to uniaxial stretching. Linear stability analysis is carried out for a number of different constitutive models, namely the Johnson–Segalman, Giesekus, Phan–Thien–Tanner, and FENE–CR. Our analysis shows that stability is controlled by the competing effects of surface tension which is destabilizing and axial normal stress which is stabilizing. Numerical simulations of the model equations are used to check the prediction of linear analysis. Results obtained agree with experimental observations.

1 Introduction

Extensional dominated flow of viscoelastic fluids are encountered in many practical situations (e.g. fiber spinning, spray and atomization, and extensional rheometry) [1, 2, 3]. Understanding the extensional behavior of such fluids and being able to accurately measure their extensional properties is therefore vitally important. One such property of interest is the extensional viscosity. For Newtonian fluids this quantity is three times the shear viscosity. For viscoelastic fluids however, the situation is more complex. Another property of practical interest is how easily such a thread will rupture when elongated. Here also, viscoelastic fluids sometimes exhibit behavior quite different from Newtonian fluids. Whereas a viscous Newtonian thread tends to break as a result of necking instability, certain viscoelastic fluids display different failure characteristics [4].

Stability of viscous threads has been extensively studied. Analysis of capillary instability go back to the linear stability of Rayleigh [5], Taylor [6] and Tomotika [7]. For a detailed bibliography see the review article of Eggers [8]. Linear stability analysis of of viscoelastic filaments in extension has been studied by Chang and Lodge [9], Lagnado et al. , [10] and Olagunju [11], for the Oldroyd–B model; and by Ide and White [12] and Forest and Wang [13] the Maxwell model. In this paper we consider the linear stability of a slender viscoelastic filament undergoing uniaxial stretching for a number of different constitutive models.

As a model for studying the extensional stability of viscoelastic threads, we consider the filament stretching device pioneered by Sridhar and co-workers [4, 14, 15, 16]. The main use of this device is for measuring the extensional properties of viscoelastic fluids. The goal is to generate in the device a flow that is as close to ideal uniaxial elongation as possible. However due to edge and capillary effects such ideal kinematics is not always attainable. Both experimental and numerical simulations have shown that near-ideal kinematics can be generated only for strain-hardening fluids [11, 17, 18]. For weakly strain-hardening fluids, pronounced necking causes the deformation to depart significantly from ideal uniaxial elongation [19]. In [11], Olagunju analyzed the stability of uniaxial extension of an Oldroyd-B thread. He showed that the flow is stable (unstable) if the Deborah number, $De > (<=) 0.5$. This conclusion is consistent with 2-D numerical simulations reported by Yao and McKinley [18].

In this paper, we examine the stability of viscoelastic threads governed by a number of constitutive models. Specifically, we will consider the Johnson-Segalman, Giesekus, Phan-Thien-Tanner, and the FENE-CR models. These models contain a single nonlinear parameter, in addition to the linear viscoelastic parameters. For a comparison of constitutive models of viscoelastic fluids in uniaxial elongation see [20, 21].

2 Governing Equations

Consider a cylindrical fluid column placed between two coaxial circular plates of radius a and initial separation h . Suppose that the bottom plate is fixed and that the column is stretched by moving the top plate. Let the gap between the plates at time \tilde{t} be $\tilde{H}(\tilde{t})$, so that the top plate moves with a velocity $\tilde{H}'(\tilde{t})$ in the axial direction. Our goal is to study the dynamics of the deformation in the column when the plates are separated at an exponential rate as in certain extensional rheometers [18]. In particular we take $\tilde{H} = h e^{\dot{\epsilon}_0 \tilde{t}}$, where $\dot{\epsilon}_0$ is the constant stretch rate. We wish to determine if the deformations approach ideal uniaxial elongation at any point in the column and what factors enhance or inhibit the attainment of this ideal kinematics.

In the following discussion a cylindrical coordinate system $(\tilde{r}, \theta, \tilde{z})$ will be used. The equations of motion are:

$$(2.1) \quad \nabla \cdot \tilde{\mathbf{v}} = \mathbf{0},$$

$$(2.2) \quad \tilde{\rho} \left(\frac{\partial \tilde{\mathbf{v}}}{\partial \tilde{t}} + \tilde{\mathbf{v}} \cdot \nabla \tilde{\mathbf{v}} \right) = -\nabla \tilde{p} + \nabla \cdot \tilde{\mathbf{T}}.$$

The above system of equations is to be solved subject to no slip conditions at the solid boundaries:

$$(2.3) \quad \tilde{\mathbf{v}} = \mathbf{0} \quad \text{on} \quad \tilde{z} = 0,$$

$$(2.4) \quad \tilde{v}_{\tilde{r}} = v_{\theta} = 0, \tilde{v}_{\tilde{z}} = \tilde{H}' \quad \text{on} \quad \tilde{z} = \tilde{H}.$$

Here $\tilde{\mathbf{v}}$ is the velocity vector, $\tilde{\mathbf{T}}$ is the stress tensor, and \tilde{p} is the pressure. In addition, we have the following conditions at the fluid air interface $\tilde{r} =$

$$\tilde{f}(\tilde{t}, \tilde{z}),$$

$$(2.5) \quad \frac{\partial \tilde{f}}{\partial \tilde{t}} + \tilde{\mathbf{v}} \cdot \nabla \tilde{f} = 0,$$

$$(2.6) \quad \mathbf{T} \cdot \mathbf{n} = (2\sigma\mathcal{H} - p_a)\mathbf{n}.$$

where σ is the surface tension, p_a is the ambient pressure and \mathcal{H} the mean curvature of the free surface.

3 Constitutive equations

In order to be able to solve the problem posed in equation (2.1)–(2.4), we must prescribe the relation between the stress and the strain. This relation is provided by the constitutive equation. In this paper we consider a number of different rheological models; specifically the Johnson–Segalman, Giesekus, Phan–Thien–Tanner (PTT), and FENE–CR models. These models contain a single adjustable nonlinear parameter, besides the linear viscoelastic parameters. While the Oldroyd-B and Johnson–Segalman models exhibit singularities in the steady state extensional stress, the others predict finite steady states at large strains [3].

The extra stress can be decomposed as

$$(3.1) \quad \tilde{\mathbf{T}} = 2\eta_s \mathbf{D} + \tilde{\boldsymbol{\tau}}.$$

Except for the FENE–CR model, $\tilde{\boldsymbol{\tau}}$ satisfies the following equation

$$(3.2) \quad \tilde{\boldsymbol{\tau}} + \mathbf{F}(\tilde{\boldsymbol{\tau}}, \mathbf{D}) + \lambda \left[\frac{\partial \tilde{\boldsymbol{\tau}}}{\partial \tilde{t}} + \tilde{\mathbf{v}} \cdot \nabla \tilde{\boldsymbol{\tau}} - (\nabla \tilde{\mathbf{v}})^T \cdot \tilde{\boldsymbol{\tau}} - \tilde{\boldsymbol{\tau}} \cdot (\nabla \tilde{\mathbf{v}}) \right] = 2\eta_p \mathbf{D},$$

where

$$\mathbf{D} \equiv \frac{1}{2}[(\nabla \tilde{\mathbf{v}}) + (\nabla \tilde{\mathbf{v}})^T],$$

and \mathbf{F} depends on the constitutive model. Here λ is the relaxation time, while η_s and η_p are solvent and polymer viscosities respectively. Equation (3.2) reduces to the Oldroyd–B model when $\mathbf{F} = 0$. The function $\mathbf{F}(\tilde{\boldsymbol{\tau}}, \mathbf{D})$ is defined for each model as follows.

Johnson–Segalman [22]

$$(3.3) \quad \mathbf{F} = \alpha\lambda(\mathbf{D} \cdot \tilde{\boldsymbol{\tau}} + \mathbf{D} \cdot \tilde{\boldsymbol{\tau}}),$$

Phan–Thien–Tanner (PTT) [23, 24]

$$(3.4) \quad \mathbf{F} = \tilde{\boldsymbol{\tau}} \left(\exp\left[\frac{\alpha\lambda}{\eta_p} \text{tr}(\tilde{\boldsymbol{\tau}})\right] - 1 \right),$$

Giesekus [25, 26]

$$(3.5) \quad \mathbf{F} = \frac{\alpha\lambda}{\eta_p} \tilde{\boldsymbol{\tau}} \cdot \tilde{\boldsymbol{\tau}}.$$

The expression $\text{tr}(\tilde{\boldsymbol{\tau}})$ denotes the trace.

For the FENE–CR model [27] the extra stress is given in terms of the configuration tensor $\tilde{\mathbf{A}}$ as

$$(3.6) \quad \tilde{\boldsymbol{\tau}} = \frac{\eta_p}{\lambda} \left[\frac{\tilde{\mathbf{A}}}{1 - \text{tr}(\tilde{\mathbf{A}})/L^2} - \mathbf{I} \right]$$

where $\tilde{\mathbf{A}}$ satisfies

$$(3.7) \quad \lambda \left(\frac{\partial \tilde{\mathbf{A}}}{\partial t} + \tilde{\mathbf{v}} \cdot \nabla \tilde{\mathbf{A}} - (\nabla \tilde{\mathbf{v}})^T \tilde{\mathbf{A}} - \tilde{\mathbf{A}} \nabla \tilde{\mathbf{v}} \right) + \frac{\tilde{\mathbf{A}}}{1 - \text{tr}(\tilde{\mathbf{A}})/L^2} = \mathbf{I}.$$

Here, \mathbf{I} is the identity matrix and L is the extensibility parameter. This model reduces to the Oldroyd–B model in the limit as $L \rightarrow \infty$.

4 One-dimensional model

In order to facilitate the analysis we use the thin filament equations derived by Olagunju [11] for axially symmetric threads. This model assumes that inertia and gravity are small and can be neglected. In situations of practical interest it has been shown that these assumptions are reasonable. One-dimensional thin-filament equations have been used in the study of fiber spinning, and jet breakup [28, 29, 30, 31, 32]. We nondimensionalize as follows,

$$(4.1) \quad \tilde{r} = ar, \quad \tilde{z} = h\xi/H, \quad \tilde{t} = t/\dot{\epsilon}_0, \quad \tilde{f} = af,$$

$$(4.2) \quad (\tilde{v}_r, \tilde{v}_z) = \dot{\epsilon}_0(au, hH'w),$$

$$(4.3) \quad p = \eta_0\dot{\epsilon}_0p, \quad \tilde{\tau}_{\tilde{r}\tilde{r}} = \eta_0\dot{\epsilon}_0r\tau_{11}, \quad \tilde{\tau}_{\tilde{z}\tilde{z}} = \eta_0\dot{\epsilon}_0\tau_{33}.$$

Here $\tilde{r} = \tilde{f}$ is the equation of the free surface. The dimensionless time, $t = \dot{\epsilon}_0\tilde{t}$, is the Hencky strain.

The functions w, p, τ_{11} and τ_{33} are all independent of r . It follows then that

$$(4.4) \quad u = -\frac{r}{2} \frac{\partial w}{\partial \xi}.$$

Next we introduce new independent variables

$$(4.5) \quad W = w - \xi, \quad \phi = \ln f.$$

After eliminating the pressure, the governing equations become

$$(4.6) \quad 3(1 - \beta) \frac{\partial^2 W}{\partial \xi^2} = -[6(1 - \beta)(1 + \frac{\partial W}{\partial \xi}) + \text{Ca}^{-1}e^{-\phi} + 2(\tau_{33} - \tau_{11})] \frac{\partial \phi}{\partial \xi} - \frac{\partial \tau_{33}}{\partial \xi} + \frac{\partial \tau_{11}}{\partial \xi},$$

$$(4.7) \quad \frac{\partial \phi}{\partial t} = -\frac{1}{2} - W \frac{\partial \phi}{\partial \xi} - \frac{1}{2} \frac{\partial W}{\partial \xi},$$

$$(4.8) \quad \tau_{11} + F1(W, \tau_{11}, \tau_{33}) \\ + \text{De} \left(\frac{\partial \tau_{11}}{\partial t} + \tau_{11} + W \frac{\partial \tau_{11}}{\partial \xi} + \tau_{11} \frac{\partial W}{\partial \xi} \right) = -\beta \left(1 + \frac{\partial W}{\partial \xi} \right),$$

$$(4.9) \quad \tau_{33} + F2(W, \tau_{11}, \tau_{33}) \\ + \text{De} \left(\frac{\partial \tau_{33}}{\partial t} - 2\tau_{33} + W \frac{\partial \tau_{33}}{\partial \xi} - 2\tau_{33} \frac{\partial W}{\partial \xi} \right) = 2\beta \left(1 + \frac{\partial W}{\partial \xi} \right),$$

with boundary conditions

$$(4.10) \quad W = 0 \text{ on } \xi = 0, 1.$$

The dimensionless quantities appearing above are the Deborah number $\text{De} = \lambda \dot{\epsilon}_0$, the capillary number $\text{Ca} = a \eta_0 \dot{\epsilon}_0 / \sigma$, and the retardation parameter $\beta = \eta_p / (\eta_s + \eta_p)$.

The functions $F1$ and $F2$ for the different constitutive equations are given below.

Johnson–Segalman

$$(4.11) \quad F1 = -\alpha \text{De} \tau_{11} \left(1 + \frac{\partial W}{\partial \xi} \right), \\ F2 = 2\alpha \text{De} \tau_{33} \left(1 + \frac{\partial W}{\partial \xi} \right).$$

Phan–Thien–Tanner (PTT)

$$(4.12) \quad F1 = \tau_{11} \left(\exp \left[\frac{\alpha \text{De}}{\beta} (2\tau_{11} + \tau_{33}) \right] - 1 \right), \\ F2 = \tau_{33} \left(\exp \left[\frac{\alpha \text{De}}{\beta} (2\tau_{11} + \tau_{33}) \right] - 1 \right).$$

Giesekus

$$(4.13) \quad \begin{aligned} F1 &= \frac{\alpha \text{De}}{\beta} \tau_{11}^2, \\ F2 &= \frac{\alpha \text{De}}{\beta} \tau_{33}^2. \end{aligned}$$

FENE-CR

For this model we have in place of equations (4.9) and (4.10), the following equations

$$(4.14) \quad \begin{aligned} A_{11} + g \text{De} \left[\frac{\partial A_{11}}{\partial t} + W \frac{\partial A_{11}}{\partial \xi} + (1 + A_{11}) \left(1 + \frac{\partial W}{\partial \xi} \right) \right] &= 0, \\ A_{33} + g \text{De} \left[\frac{\partial A_{33}}{\partial t} + W \frac{\partial A_{33}}{\partial \xi} - 2(1 + A_{33}) \left(1 + \frac{\partial W}{\partial \xi} \right) \right] &= 0, \end{aligned}$$

where

$$\begin{aligned} g &= 1 - \frac{3 + 2A_{11} + A_{33}}{L^2}, \\ \tau_{11} &= \frac{\beta}{\text{De}} \frac{A_{11}}{g}, \end{aligned}$$

and

$$\tau_{33} = \frac{\beta}{\text{De}} \frac{A_{33}}{g}.$$

Here we have $A_{11} = \tilde{\mathbf{A}}_{rr} - 1$ and $A_{33} = \tilde{\mathbf{A}}_{zz} - 1$.

The 1-D equations (4.6)–(4.10) do not satisfy all the boundary conditions at the rigid end-plates. However, all the conditions at the fluid-air interface are satisfied. Consequently, we expect the model to give a good approximation to the deformation in the central portion of the filament. In [11], it was shown that the results for the Oldroyd-B model agree very well with numerical results of the full two-dimensional axisymmetric problem [17, 18].

5 Stability of ideal uniaxial extension

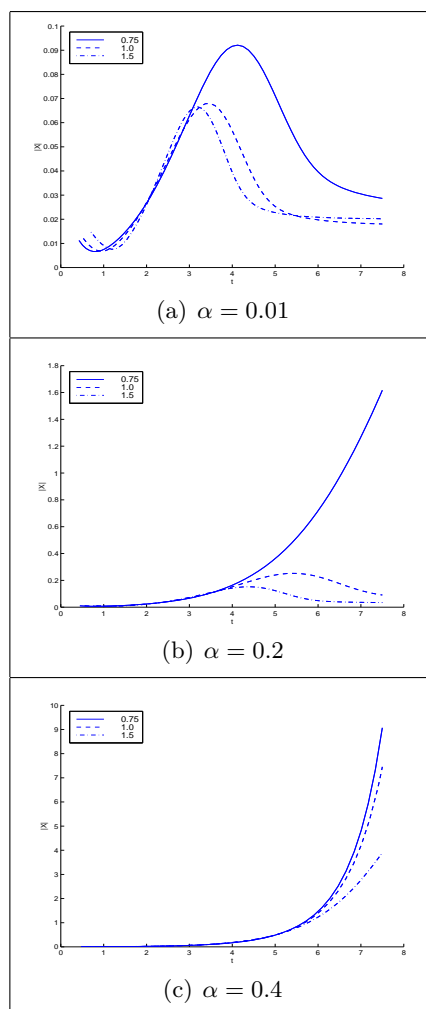


Figure 1: Solution of linearized equations of the Johnson–Segalman model for $\beta = 0.08$, $Ca = 21.0$, and selected values of α and De .

One solution of equations (4.6)–(4.10) is $W = 0$, and $\phi = -\frac{t}{2}$, which corresponds to ideal uniaxial elongation. The normal stresses $\tau_{11}(t)$ and $\tau_{33}(t)$ satisfy two decoupled ordinary differential equations which are easily

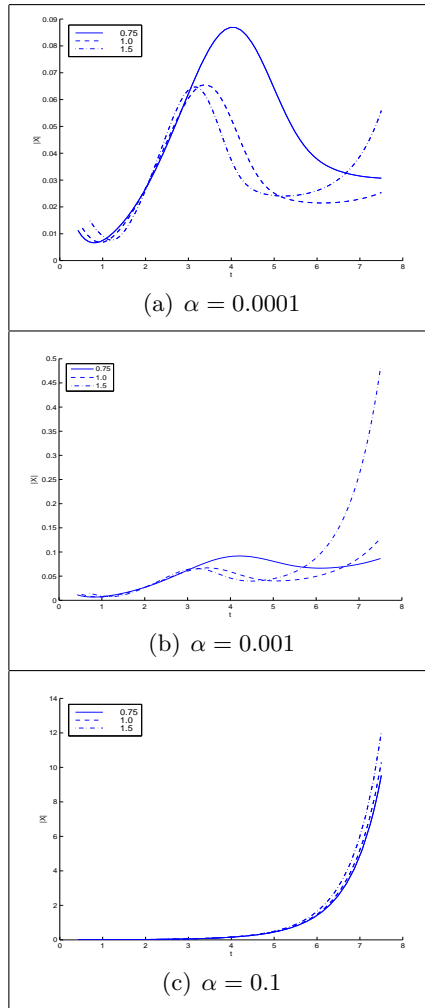


Figure 2: Solution of linearized equations of the Giesekus model for $\beta = 0.08$, $\text{Ca} = 21.0$, and selected values of α and De .

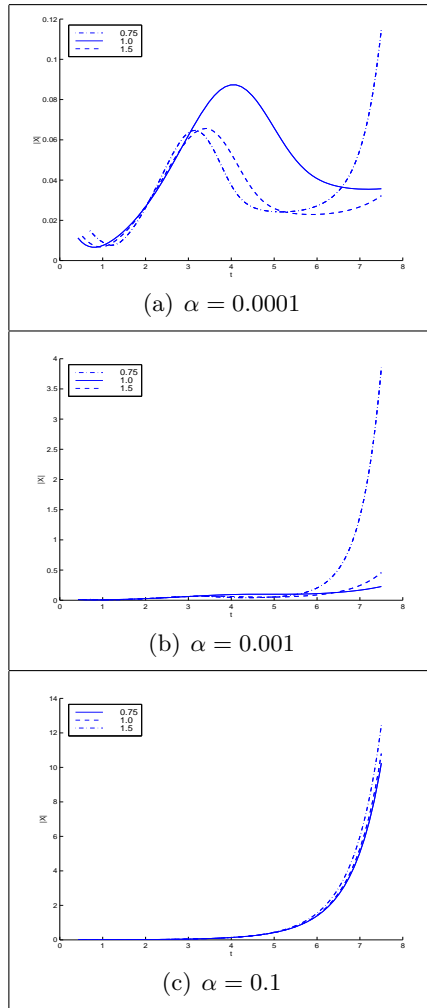


Figure 3: Solution of linearized equations of the PTT model for $\beta = 0.08$, $Ca = 21.0$, and selected values of α and De .

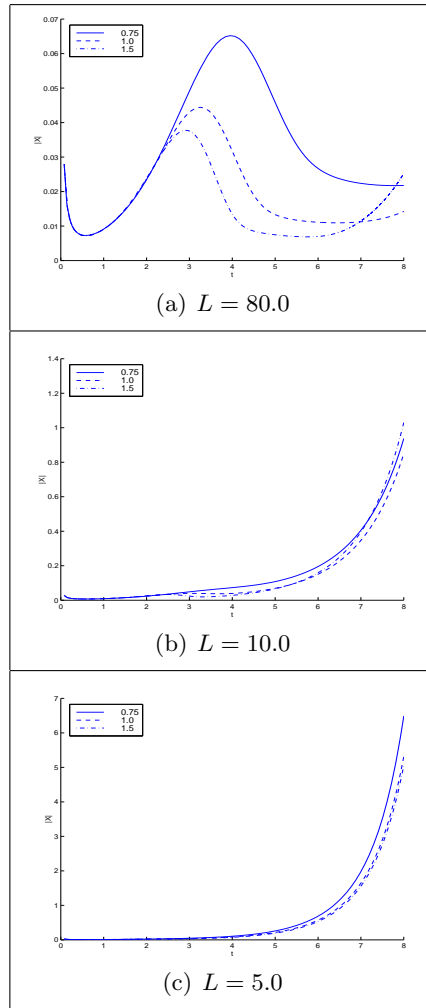


Figure 4: Solution of linearized equations of the FENE–CR model for $\beta = 0.08$, $Ca = 21.0$, and selected values of α and De .

solved. For the Oldroyd–B model it was shown in [11] that this solution is unstable if the Deborah number De is less than or equal to 0.5, and stable if $De > 0.5$. Here we examine the linear stability of this base flow for each of the constitutive models given above. We introduce small perturbations to the base flow and linearize the governing equations in the usual way. If the solution of the linearized equations grows with time then we say that the base flow is unstable, otherwise it is stable. Calculations were done for selected values of the nonlinear parameters α and L and the results are shown in Figures 1– 4 where the norm of the perturbation relative to the base flow $|X|$ is plotted against time t .

As the figures indicate, increasing the nonlinear parameter destabilizes the base flow. This means that the Oldroyd-B model is the most stable of all the models. For this reason our calculations were restricted to values of Deborah number for which the Oldroyd–B model is stable i.e. $De > 0.5$. For all values of Deborah number considered, the flow is stable if α or L^{-1} is sufficiently small and unstable otherwise. Note that perturbations increase initially due to surface tension. For small α , this destabilizing effect is overcome by the large transient axial stresses which cause the filament to strain–harden. As a result the flow is restabilized and the filament deforms almost uniaxially. However, as α increases and nonlinear effects become important, the amount of strain–hardening is sufficiently curtailed that elastic stresses are unable to overcome the destabilizing effect of surface tension. Therefore, a small initial defect will grow and ultimately cause the thread to

fail in finite time like a Newtonian fluid. For a fixed value of the nonlinear parameter ($\alpha \neq 0$, $L \neq \infty$), linear theory also shows that the flow becomes less stable as the Deborah number De increases. Increasing the Deborah number also increases the importance of nonlinear terms which tend to destabilize the flow. This is in contrast to the Oldroyd–B model for which the reverse is the case where an increase in Deborah number produces an increase in the axial normal stresses which leads to greater strain–hardening.

6 Numerical simulation

In this section we solve the nonlinear equations (4.6)–(4.10) numerically. Equation (4.6) can be solved explicitly for W (see [11]). Thus we are left with three equations which we solve using a finite difference scheme. The equations were discretized using a third–order upwind scheme in space and a second order Runge–Kutta scheme in time. For the retardation parameter β , and the capillary number Ca , we used the data from the experiments and numerical simulations of McKinley *et al.* [4, 18]. We took an initial free surface profile $f(0, \xi) = 1 - e\xi(1 - \xi)$ where e is small so that initially the free surface is a small perturbation of a cylinder. The stresses are taken to be zero initially.

In Figure 5, we plot the axial velocity w vs. the spatial variable ξ at the end of the simulation, and the extension rate rate $\dot{\epsilon} \equiv -2\frac{\partial\phi}{\partial t}$, of the mid–filament radius for selected values the nonlinear parameters α and L . For the Johnson–Segalman model, Figure 5(a), we see that axial velocity approaches

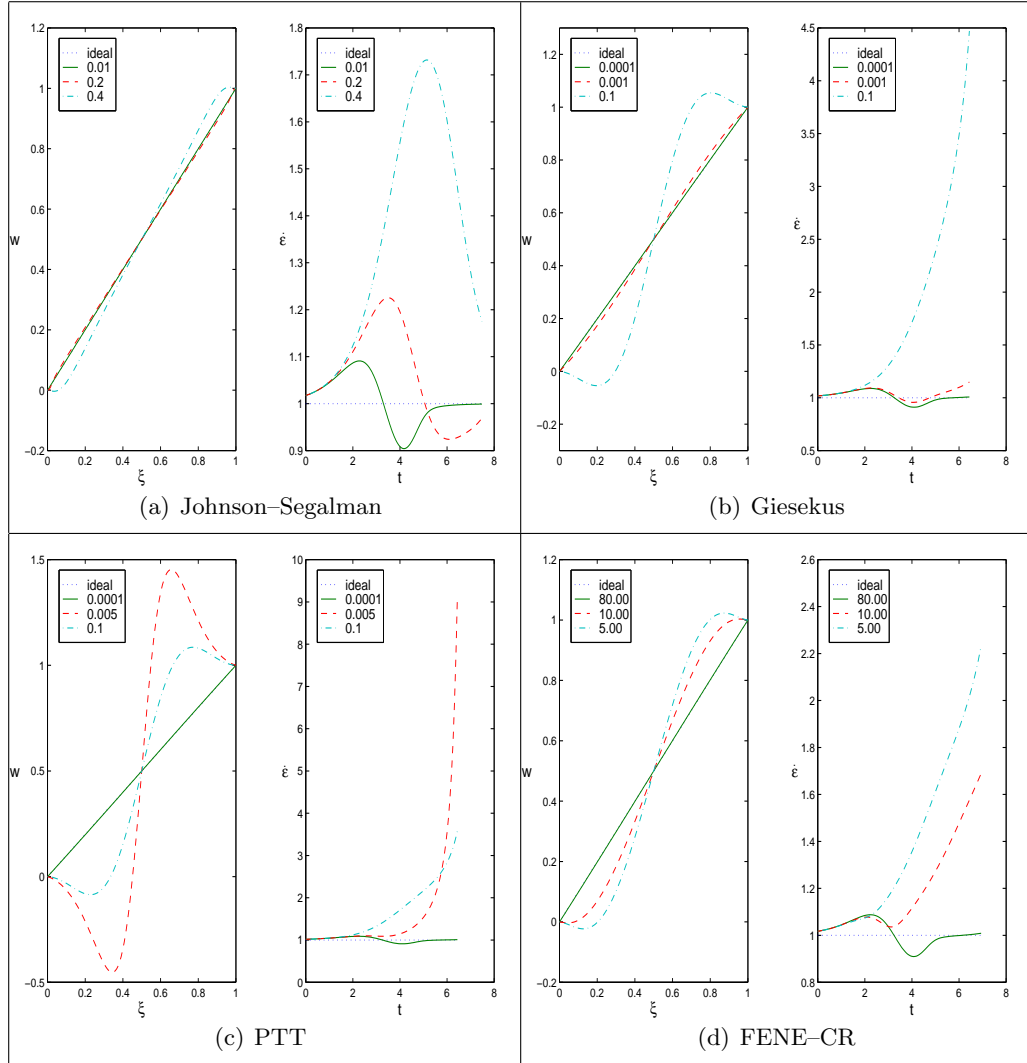


Figure 5: Axial velocity and the extension rate at the mid-filament radius, for $De = 1.0$, $\beta = 0.08$, $Ca = 21.0$, $e = 0.1$, and selected values of α and L

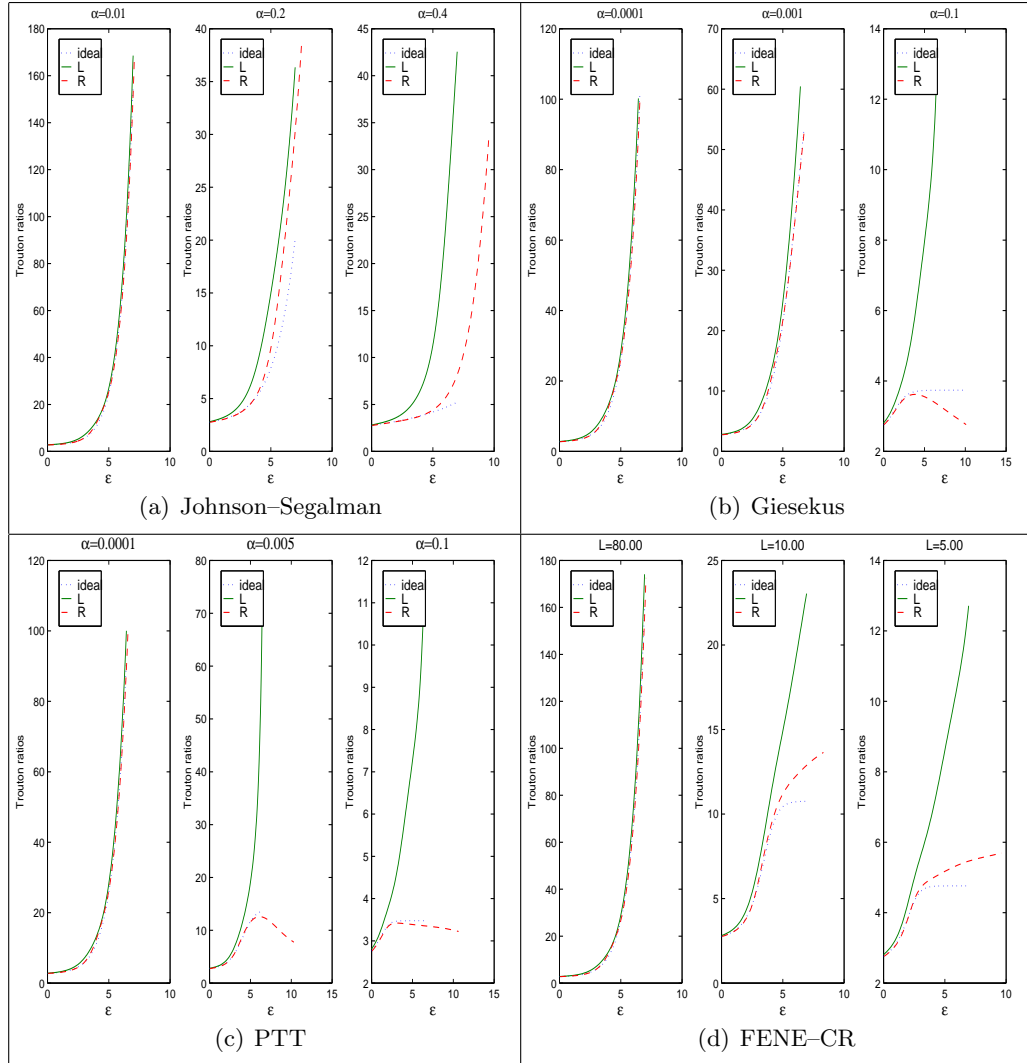


Figure 6: Trouton ratios for $De = 1.0$, $\beta = 0.08$, $Ca = 21.0$, $e = 0.1$, and selected values of α and L .

uniaxial extension $w = \xi$, at the end of the simulation except for $\alpha = 0.4$. This is also evident from the plot of $\dot{\epsilon}$ vs t . For $\alpha = 0.4$ the extension rate increases with strain so that necking is accentuated. However, for smaller values of α , the extension rate decreases with strain and approaches ideal uniaxial extension. The results for the Giesekus and PTT models depicted in Figures 5 (b, c) respectively, show that for α very small, the flow approaches uniaxial extension but as α increases we see greater departure from ideal kinematics for reasons explained above. For the FENE–CR model, Figure 5(d), the deformation is very close to uniaxial extensional provided that the extensibility parameter is sufficiently large. These observations are all consistent with the results of linear stability analysis given above. In Figure 6, we show Trouton ratios based on the imposed stretch rate (L), and on the extension rate at the mid-filament radius (R). We also show the Trouton ratio for pure uniaxial extension for the same parameter values (dotted curve). In all cases the three calculations agree very well when the deformation approaches uniaxial extension. When significant departure from uniaxial elongation occurs, the Trouton ratios based on the stretch rate is unable to predict the correct values of the steady state extensional viscosity. Note that approach to uniaxial flow is marked by large transient extensional viscosities, a sign of strain hardening. As the nonlinear parameter increases the filament does not show significant strain–hardening. Consequently, the initial defect in the filament profile becomes more pronounced with increasing strain. This can be clearly seen from Figure 7 which depicts the shape

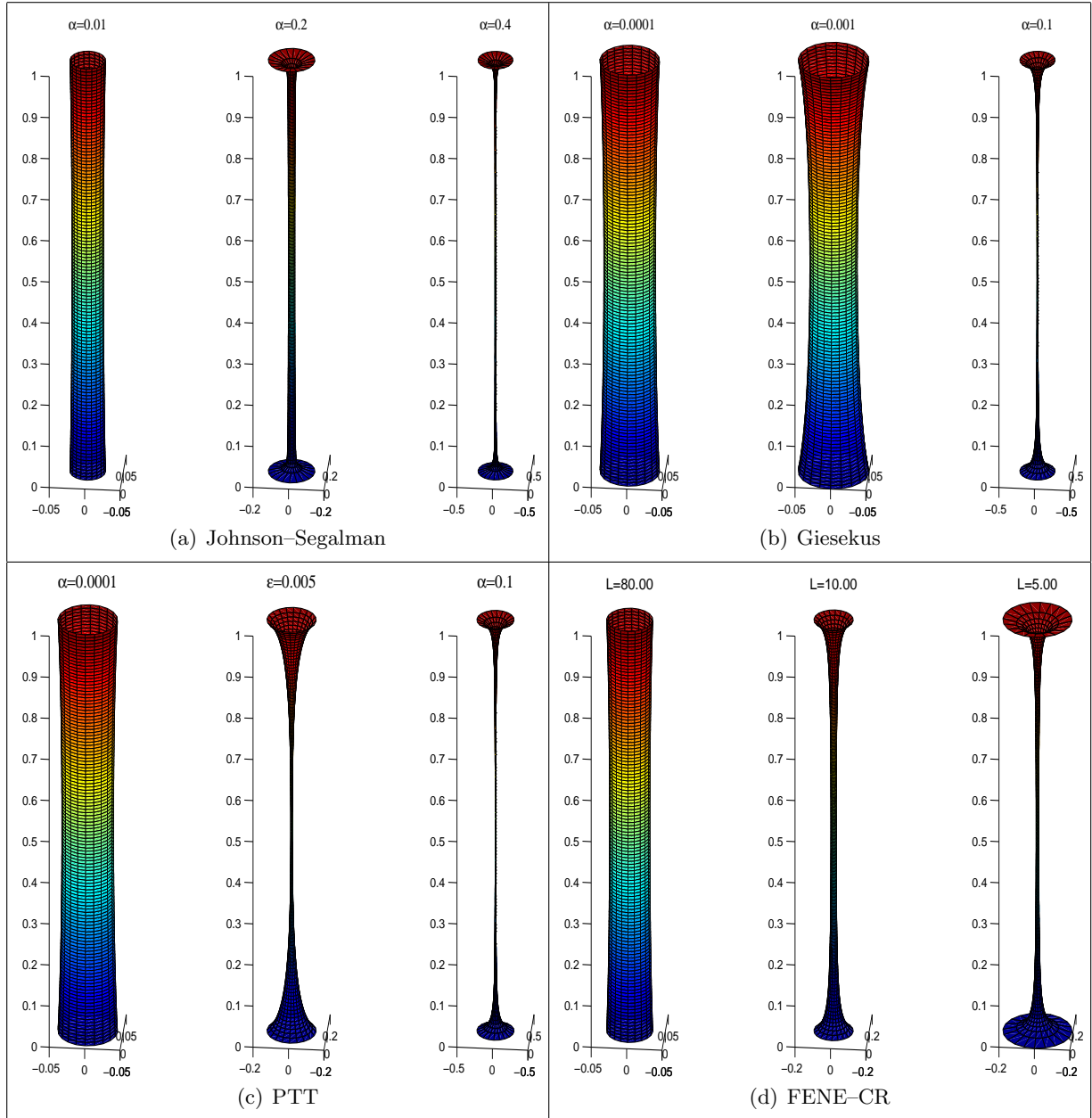


Figure 7: Filament at the end of simulation, for $De = 1.0$, $\beta = 0.08$, $Ca = 21.0$, $e = 0.1$, and selected values of α , and L .

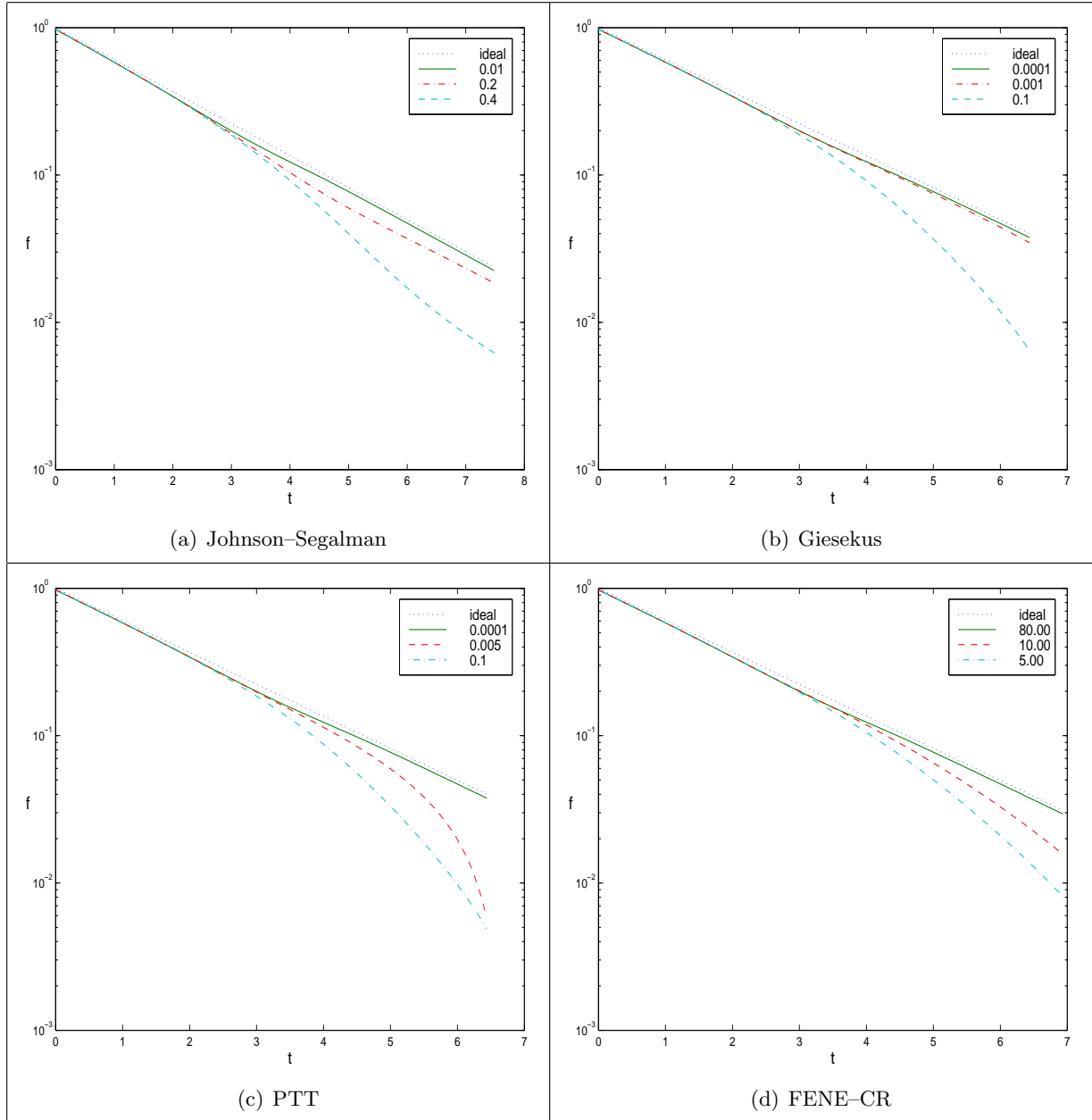


Figure 8: Evolution of mid-filament radius f , for $De = 1.0$, $\beta = 0.08$, $Ca = 21.0$, $e = 0.1$, and selected values of α , and L .

of the filament at different stages in the deformation. All calculations for each model were done with the same initial conditions and were terminated at the same time.

For small (large) values of $\alpha (L)$, the initial defect in the filament heals itself to a large extent as the fluid begins to strain-harden. This can also be seen from Figure 8 which shows the evolution of the mid-filament radius. These results agree with the finite element simulations of Sizaire and Legat [17], for a FENE-CR thread. Similarly, the numerical simulations of Yao and McKinley [18] show that when initial aspect ratio is not too small (so that the filament was a little slender initially) the evolution of the mid-plane radius approaches uniaxial kinematics with increasing Hencky strain. Their simulations were done with an Oldroyd-B fluid. This shows that our one-dimensional model gives an accurate description of the deformation in the middle portion of the filament in the stretching device.

7 Conclusion

A thin filament model is used to analyze the stability of viscoelastic filaments under uniaxial elongation for a number of constitutive equations. We have considered the Johnson-Segalman, Giesekus, Phan-Thien Tanner and FENE-CR models. In addition to the usual linear viscoelastic parameters these models contain an additional non-linear parameter $\alpha (L$ for the FENE-CR model). Stability is controlled by the competing effects of surface tension and elastic normal stresses. Linear stability analysis shows

that the filament is stable if $\alpha (L)$ is sufficiently small (large), and unstable otherwise. Initially capillary forces dominate and perturbations grow exponentially. However, for very small values of α , there is a sharp increase in the axial normal stresses causing the filament to significantly strain-harden. If the degree of strain hardening is sufficiently large, the destabilizing effect of surface tension is overcome and the initial defect partially heals itself. In such a case the filament deforms almost uniaxially. On the other hand if α is not small the amount of strain hardening is not sufficient to overcome capillary instability and any initial defect will grow and lead to a failure of the thread just like a Newtonian thread. Numerical solution of the nonlinear model equations were also obtained which confirm the prediction of linear theory. These results agree with experiments and numerical simulations.

References

- [1] Petrie, C. J., *Elongational Flows*, Pitman, London, 1979.
- [2] Walters, K., *Rheometry*, Chapman & Hall, London, 1975.
- [3] Bird, R. B., Armstrong, R. C., and Hassager, O., *Dynamics of Polymeric Liquids*, Vol. 1 Fluid Mechanics, 3rd ed., John Wiley & Sons, 1987.
- [4] Spiegelberg, S. H., Ables, D. C., and McKinley, G. H., The role of end effects on measurements of extensional viscosity in filament stretching rheometers, *J. Non-Newtonian Mech.*, 64 (1996), 229–267.
- [5] Rayleigh, Lord, On the instability of a cylinder of viscous liquid under capillary force, *Phil. Mag.*, 34 (1892), pp. 145–154.
- [6] Taylor, G. I., The formation of emulsions in definable fields of flow, *Proc. Roy. Soc. A* 146 (1934), pp. 501–523.
- [7] Tomotika, S., On the instability of a cylindrical thread of a viscous liquid surrounded by another viscous fluid, *Proc. Roy. Soc. A* 150 (1935), pp. 322–337.
- [8] Eggers, J., Nonlinear dynamics and breakup of free-surface flows, *Rev. Mod. Phys.*, 69(3), (1997), pp. 865–929.

- [9] Chang, H., and Lodge, A. S., A possible mechanism for stabilizing elongational flow in certain polymeric liquids at constant temperature and composition, *Rheol. Acta* 10 (1971), pp. 448–449.
- [10] Lagnado, R. R., Phan–Thien, N., and Leal, G., The stability of two-dimensional linear flows of an Oldroyd–type fluid, *J. Non–Newtonian Fluid Mech.*, 18 (1985), pp. 25–59.
- [11] Olagunju, D. O., A 1–D theory for extensional deformation of a viscoelastic filament under exponential stretching, *J. Non–Newt. Fluid. Mech.*, 87 (1999) pp. 27–46.
- [12] Ide, Y., and White, J. L., Investigation of failure during elongational flow of polymer melts, *J. Non–Newt. Fluid Mech.*, 2 (1977), pp. 281–298.
- [13] Forest, M. G., and Wang, Q., Dynamics of slender viscoelastic free jets, *Siam J. Applied Math.*, 54 (1994), pp. 996–1032.
- [14] Tirtaatmadja, V., and Sridhar, T., A filament stretching device for measurement of extensional viscosity, *J. Rheol.* 37 (1993), pp. 1081–1102.
- [15] Kroger, R., Berg, S., Delgado, A., and Rath, H. J., Stretching behavior of large polymeric and Newtonian liquid bridges in plateau simulations, *J. Non–Newt. Fluid Mech.*, 45 (1992), 385–400.

- [16] Solomon, M. J., and Muller, S. J., The transient extensional behavior of polystyrene-based Boger fluids of varying solvent quality and molecular weight, *J. Rheol.*, 40 (1996), 837–856.
- [17] Sizaire, R., and Legat, V., Finite element simulation of a filament stretching extensional rheometer, *J. Non-Newton. Fluid Mech.*, 71 (1997). 89–107.
- [18] Yao, M., and McKinley, G. H., Numerical simulation of extensional deformations of viscoelastic liquid bridges in filament stretching devices, *J. Non-Newton. Fluid Mech.*, 74 (1998), pp. 47–88.
- [19] Yao, M., Spiegelberg, S. H., and McKinley, G. H., Fluid dynamics of weakly strain-hardening fluids in filament stretching devices, submitted.
- [20] Khan, S. A., and Larson, R. G., Comparison of simple constitutive equations for polymer melts in shear and biaxial and uniaxial extensions, *J. Rheol.* 31(3) (1987), pp. 207–234.
- [21] Tirtaatmadja, V., and Sridhar, T., Comparison of constitutive equations for polymer solutions in uniaxial extension, *J. Rheol.*, 39(6) (1995), pp.1133–1160.
- [22] Johnson, M. W. Jr., Segalman, D., *J. Non-Newton Fluid Mech.*, 2 (1977) pp. 225.

- [23] Phan–Thien, N., and Tanner, R. I., *J. Non–Newt Fluid Mech.*, 2 (1977) pp. 353.
- [24] Phan–Thien, N., *J. Rheol.* 22 (1978) pp. 259.
- [25] Giesekus, H., *Rheol Acta* 5 (1966) pp. 29.
- [26] Giesekus, H., *J. Non–Newt. Fluid Mech.*, 11 (1982) pp. 69.
- [27] Chilcott, M. D., and Rallison, J. N., Creeping flow of dilute polymer solutions past cylinders and spheres, *J. Non–Newt. Fluid Mech.*, 29 (1988) pp. 381–432.
- [28] Forest, M. G., and Wang, Q., Dynamics of slender viscoelastic free jets, *SIAM J. Appl. Math.*, 54 (4), (1994) pp. 996–1032.
- [29] Matovich, M. A., and Pearson, J. R. A., *Ind. Eng. Chem. Fundam.* 8 (1969), pp. 512–520.
- [30] Renardy, M., Some comments on the surface–tension driven breakup (or lack of it) of viscoelastic jets, *J. Non–Newt. Fluid Mech.*, 51, (1994), pp. 97–.
- [31] Schultz, W. W., Slender viscoelastic fiber flow, *J. Rheol.* 31 (8) 1987, 733–750.
- [32] Schultz, W. W. and Davis, S. H., One dimensional liquid fibers, *J. Rheol.* 26(4) 1982, pp. 331–345.

FIGURE CAPTIONS

- Figure 1: Solution of linearized equations of the Johnson–Segalman model for $\beta = 0.08$, $Ca = 21.0$, and selected values of α and De .
- Figure 1a: $\alpha = 0.01$
- Figure 1b: $\alpha = 0.2$
- Figure 1c: $\alpha = 0.4$
- Figure 2: Solution of linearized equations of the Giesekus model for $\beta = 0.08$, $Ca = 21.0$, and selected values of α and De .
- Figure 2a: $\alpha = 0.0001$
- Figure 2b: $\alpha = 0.001$
- Figure 2c: $\alpha = 0.1$
- Figure 3: Solution of linearized equations of the PTT model for $\beta = 0.08$, $Ca = 21.0$, and selected values of α and De .
- Figure 3a: $\alpha = 0.0001$
- Figure 3b: $\alpha = 0.001$
- Figure 3c: $\alpha = 0.1$
- Figure 4: Solution of linearized equations of the FENE–CR model for $\beta = 0.08$, $Ca = 21.0$, and selected values of α and De .
- Figure 4a: $\alpha = 80.01$
- Figure 4b: $\alpha = 10.0$
- Figure 4c: $\alpha = 5.0$
- Figure 5: Axial velocity and extension rate at the mid–filament radius, for $De = 1.0$, $\beta = 0.08$, $Ca = 21.0$, $e = 0.1$, and selected values of α and L .
- Figure 5a: Johnson–Segalman
- Figure 5b: Giesekus
- Figure 5c: PTT
- Figure 5d: FENE–CR

- Figure 6: Trouton ratios for $De = 1.0$, $\beta = 0.08$, $Ca = 21.0$, $e = 0.1$, and selected values of α and L .
- Figure 6a: Johnson–Segalman
- Figure 6b: Giesekus
- Figure 6c: PTT
- Figure 6d: FENE–CR
- Figure 7: Filament profile at the end of simulation for $De = 1.0$, $\beta = 0.08$, $Ca = 21.0$, $e = 0.1$, and selected values of α and L .
- Figure 7a: Johnson–Segalman
- Figure 7b: Giesekus
- Figure 7c: PTT
- Figure 7d: FENE–CR
- Figure 8: Evolution of mid–filament radius for for $De = 1.0$, $\beta = 0.08$, $Ca = 21.0$, $e = 0.1$, and selected values of α and L .
- Figure 8a: Johnson–Segalman
- Figure 8b: Giesekus
- Figure 8c: PTT
- Figure 8d: FENE–CR